Journal of Pharmaceutical and Biomedical Analysis 237 (2024) 115750

Contents lists available at ScienceDirect

Journal of Pharmaceutical and Biomedical Analysis

journal homepage: www.journals.elsevier.com/journal-of-pharmaceutical-and-biomedical-analysis

Selective inhibition of indoleamine and tryptophan 2,3-dioxygenases: Comparative study on kynurenine pathway in cell lines *via* LC-MS/MS-based targeted metabolomics

Salvatore Villani [1], Silvia Fallarini [1], Sarah Jane Rezzi, Rita Maria Concetta Di Martino, Silvio Aprile, Erika Del Grosso [*]

Department of Pharmaceutical Sciences, University of Piemonte Orientale, Largo Donegani 2, 28100, Novara, Italy

ARTICLE INFO

Keywords:
Kynurenine pathway
LC-MS/MS
Method validation
HIDO1
TDO
Targeted-metabolomics

ABSTRACT

In the last decade, the kynurenine pathway, which is the primary metabolic route for tryptophan (TRP) catabolism, has sparked great interest in the pharmaceutical sciences due to its role in immune regulation and cancer immunoediting. In this context, the development of cell-based assays might represent a tool to: i) characterize the cell secretome according to cell types; ii) gain more insight into the role of kynurenines in different disease scenarios; iii) screen hIDO1 (human indoleamine 2,3-dioxygenase) inhibitors and evaluate their effect on downstream TRP-catabolizing enzymes. This paper reports a validated Liquid Chromatography with tandem mass spectrometry (LC-MS/MS) method to simultaneously quantify TRP, L-kynurenine (KYN), xanthurenic acid (XA), 3-hydroxykynurenine (3OHKYN), kynurenic acid (KA), 3-hydroxyanthranilic acid (3OHAA), anthranilic acid (AA), 5-hydroxytryptamine (serotonin, 5HT) and tryptamine (TRYP) in Dulbecco's Modified Eagle and Eagle's Minimum Essential Media (DMEM and EMEM, respectively). The quantitative method was validated according to FDA, ICH and EMA guidelines, later applied: i) to assess the impact of selective inhibition of hIDO1 or hTDO (human tryptophan 2,3-dioxygenase) on the kynurenine pathway in A375 (melanoma), MDA-MB-231 (breast cancer), and U87 (glioblastoma) cell lines using multivariate analysis (MVA); ii) to determine the IC_{50} values of both well-known (*i.e.*, epacadostat, linrodostat) and the novel hIDO1 inhibitor (*i.e.*, BL5) in the aforementioned cell lines. The proposed LC-MS/MS method is reliable and robust. Furthermore, it is highly versatile and suitable for applications in the preclinical drug research and *in vitro* assays.

1. Introduction

L-Tryptophan (TRP) is one of the nine essential amino acids, which human cells must get through the diet. [1] TRP plays a key role in a number of physiological functions (*i.e.*, coordination of responses to environmental and dietary cues, cellular turnover increase) and undergoes biotransformation into bioactive molecules *via* multiple catabolic pathways, as depicted in Fig. 1. [1] It has been estimated that approximately 95% of dietary tryptophan not utilized for protein synthesis serves as a substrate for the kynurenine pathway (KP), a set of TRP degradation steps that evolves towards the generation of several neuro- and/or immune modulators and culminates in the formation of nicotinamide adenine dinucleotide (NAD+), an important cellular energy source. The first and rate-limiting step of the KP is the oxidative degradation of TRP into N-formyl-L-kynurenine (NFK), which is catalyzed by three heme-oxidoreductases, namely TRP 2,3-dioxygenase (TDO), indoleamine 2,3-dioxygenases 1 and 2 (IDO1 and IDO2). After its generation, NFK is rapidly degraded into L-kynurenine (KYN). [2]

Although hTDO and hIDO catalyze the same reaction, they show a peculiar tissue-specific localization, engage in distinct physiological functions, and are induced by different stimuli. [3] hTDO is mostly expressed in liver and secondary districts (*e.g.*, bone marrow, immune system, muscles, gastrointestinal tract, kidneys, bladder and brains). [4] On the other hand, hIDO1 is a ubiquitous protein that is basally expressed in CNS, but might be induced by proinflammatory cytokines (*e.g.*, interferon gamma (IFNγ) and interleukin 6 (IL-6)) in myeloid cells. [2] The protein expression is also promoted in dendritic, cancer and stromal cells after the interaction of cytotoxic T-lymphocyte-associated

* Corresponding author.
E-mail address: erika.delgrosso@uniupo.it (E. Del Grosso).
[1] These authors contributed equally to the paper

https://doi.org/10.1016/j.jpba.2023.115750
Received 29 June 2023; Received in revised form 22 September 2023; Accepted 22 September 2023
Available online 26 September 2023

protein 4 (CTLA4), expressed in Treg cells, with *in loco* CD80/CD86 co-stimulatory molecules. [2] Of note, hIDO1 exists in a dynamic equilibrium between two alternative forms, a heme-bound form (holo-IDO1), that is catalytically competent, and a heme-free form (apo-IDO1), whose biology and functions are still under investigation. [5]

hIDO2 is constitutively located in the liver, brain, thyroid, placenta, endometrium and testicles and has been reported to have lower affinity and catalytic efficiency for TRP than hIDO1. [6] Although hIDO1 and hIDO2 are expressed in numerous tissues, immunohistochemistry experiments have demonstrated that these enzymes are not functionally redundant. [5]

In tumors, activation of TRP catabolism by any of the TRP-degrading enzymes leads to a local generation of immunosuppressive kynurenines and TRP depletion with consequent poor immune responses. [2] Due to the role of TRP catabolism in promoting immune suppression, targeting TRP-KYN-IDO1 pathway *via* hIDO1 inhibition might represent an immunotherapy approach to aid cancer management. Over the past decade, many IDO1 inhibitors have been developed and at least 10 candidates have entered clinical trials, *e.g.* indoximod (NLG-8189) singularly or combined with checkpoint inhibitors and chemotherapy. [7] 18 clinical studies for indoximod are registered in ClinicalTrails website and, recently, the same inhibitor has been granted orphan-drug designation by the US FDA for the treatment of stage IIb to stage IV melanoma. [8]

Among hIDO1 catalytic inhibitors endowed with high selectivity over TDO and hIDO2, epacadostat (EP) is one of the most investigated compounds. Also known as INCB024360, it is an holo-IDO1 selective inhibitor characterized by the presence of a hydroxyamidine group, which is essential for forming a coordinate covalent bond with the Fe(II)

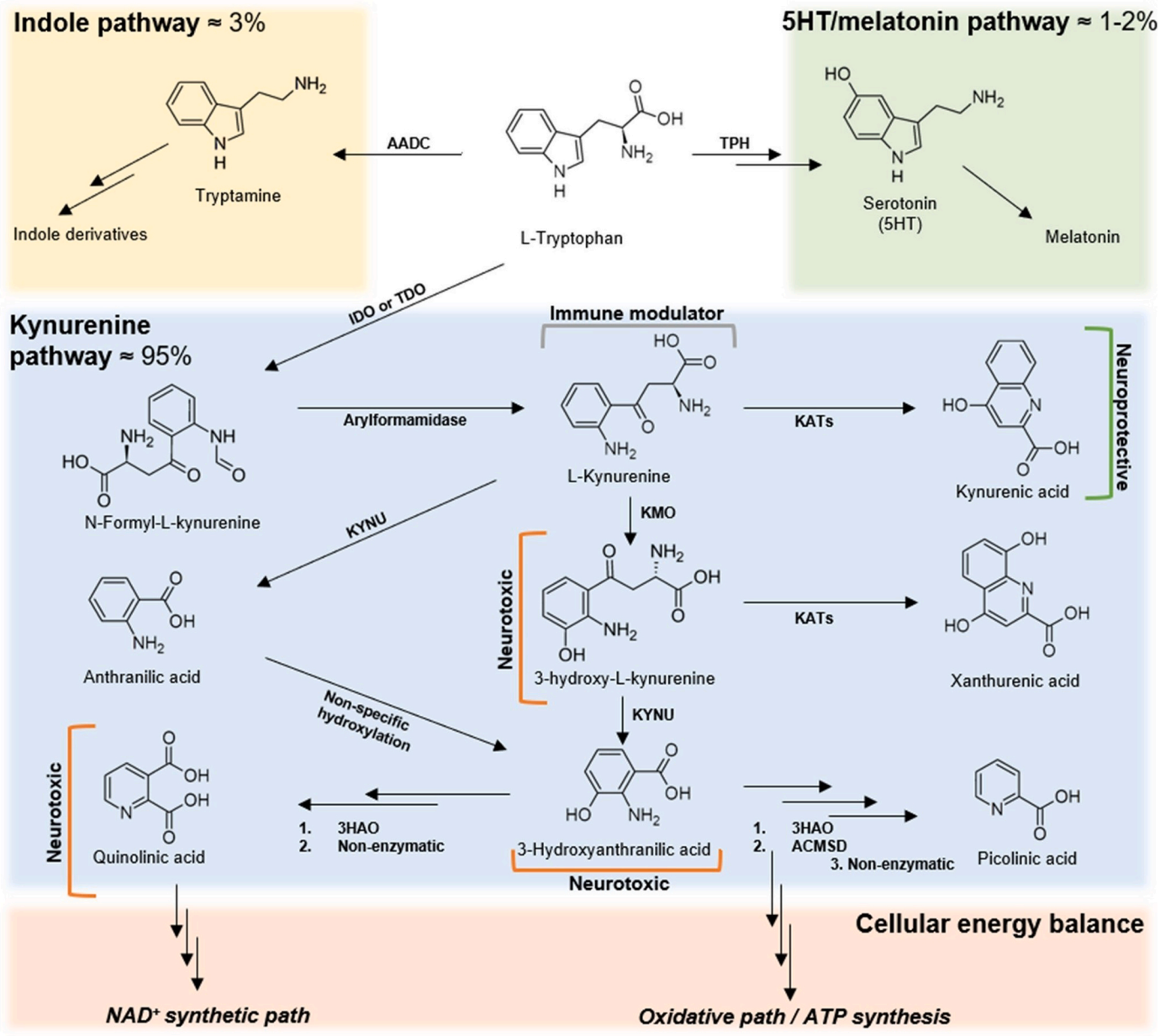

Fig. 1. Main catabolic pathways of TRP. Representation of TRP catabolism focused on the KP, and the physiological role of the generated metabolites. List of the enzyme acronyms: AADC (aromatic L-amino acid decarboxylase), TPH (TRP hydroxylase), IDO (indoleamine 2,3-dioxygenase), TDO (TRP 2,3-dioxygenase), KATs (kynurenine aminotransferases), KMO (kynurenine 3-monoxygenase), KYNU (KYNUreninase), 3HAO (3-hydroxyanthranilate oxidase), and ACMSD (amino-carboxymuconate semialdehyde decarboxylase).

of the heme. EP in its early phase I/II trials proved to: i) promote the growth of effector T and NK cells; ii) reduce the conversion of Naïve T cells into Treg; iii) induce the upregulation of CD86. [9] However, in a Phase III trial its combination with pembrolizumab failed to demonstrate superiority *versus* pembrolizumab alone in melanoma patients. [9] The unexpected results, rather than toning down the enthusiasm, raised new questions and spurred additional search for a greater understanding of hIDO1 biology, as well as for more effective molecules including a few apo-IDO1 inhibitors. [10] They bind to the apoenzyme devoid of the heme prosthetic group, preventing the formation of hIDO1 holo form. [11] One example is linrodostat (LIN), a potent and selective apo-inhibitor of hIDO1, which is able to reverse the immunosuppression system in cancer patients by inhibiting hIDO1 and reducing kynurenine levels in tumor cells. LIN has completed various Phase I/II trials but is currently undergoing further evaluation. [8]

In this scenario, the role of bioanalytical chemistry is to provide reliable and orthogonal tools to characterize and confirm the cell biology, thereby enhancing our understanding of the regulation of the KP. This, in turn, supports the preclinical investigation of novel potential therapeutics. From the analytical standpoint, the complete profiling of kynurenines is challenging due to their different physicochemical properties. In the last years, several analytical techniques have been adopted in metabolomics, such as nuclear magnetic resonance spectroscopy (NMR), gas and liquid chromatography (GC, LC) coupled with fluorescence, ultraviolet or mass spectrometry detection (FD, UV, MS). [12–16] Among these procedures, quantitative liquid chromatography with tandem mass spectrometry (qLC-MS/MS) ensures both high resolution and selectivity, with a lower risk of interferences caused by endogenous compounds. Nevertheless, one of the main challenges in quantitative LC-MS is still the matrix effect, which can either enhance or hinder the mass response of the analytes of interest. Consequently, several purification techniques, such as solid-phase extraction, liquid-liquid extraction, protein precipitation, turbulent flow chromatography, and microdialysis, are employed to clean up the samples. [17] Biological fluids such as plasma, serum and urine are the main matrices gained by *in vivo* studies, in which hIDO1 activity is measured by KYN/TRP ratio that is strictly related to the depletion of TRP. [18,19] In the realm of biological matrices, cell culture supernatants have garnered significant attention in early drug discovery and *in vitro* cancer pharmacology. This is primarily due to the fact that they are compatible with cell-based assays, which provide a more physiological environment compared to cell-free assays. Additionally, cell-based assays enable the simultaneous evaluation of various drug-like properties, including membrane permeability, toxicity, and off-target effects. Moreover, they offer improved resource efficiency compared to enzyme assays and support the utilization of cell culture media that are typically considered waste after incubation. However, the current state-of-the-art includes a limited number of published LC-MS methods dedicated to the quantification of the kynurenines in cell culture media. [14,20,21]

Regarding the quantitative analysis of kynurenine intermediates in cell culture media, the sample preparation often involves protein precipitation with organic modifiers, followed by full drying of the supernatants and subsequent reconstitution in a smaller volume. [19,21] To obtain matrix-matched calibration curves, activated charcoal treatment is applied to the matrices to remove the basal levels of kynurenines, particularly TRP and KYN, from the samples. While this pre-treatment may be necessary for biological matrices like plasma or serum due to their elevated baseline levels of TRP, KYN, and other related catabolites, it may be an additional step for media samples. [14,22] Furthermore, charcoal stripping is nonspecific and may alter the composition of the native matrices in terms of hydrophobic compounds, as well as affect salts and organic polar molecules, leading to unsatisfactory matrix similarity. [17]

From an analytical perspective, the aim of this study is to optimize an LC-MS/MS method for the rapid quantification of kynurenines by shortening the sample preparation time and by eliminating the drying and reconstitution steps. These steps, if included, can potentially amplify the matrix effect by increasing salt concentration and introducing other interferences. [17]

On the other hand, considering the application field, the scope of this investigation is to characterize the kynurenine profile in different cell lines commonly used *in vitro*, aiding in the selection of the optimal model for developing a cell-based inhibition assay and identifying systems that can differentiate activity towards IDO and TDO, thereby assessing the selectivity and potency of tested molecules in the preclinical drug research. In this context, a comparative study was carried out through multivariate analysis (MVA) based on targeted metabolomic results. The quantitative data enabled a comprehensive comparison and analysis of the TRP catabolites, providing valuable insights into the kynurenine pathway. Specifically, the simultaneous quantification of main KP metabolites was performed in culture media of three different cancer cell lines: glioblastoma (U87), breast cancer (MDA-MB-231), and melanoma (A375) before and after treatment with selective hIDO1 or TDO inhibitors. We selected two well-known potent and selective hIDO1 inhibitors: EP, an holo-inhibitor, and LIN, an apo-inhibitor. Moreover, we used the compound *N*-[[3-(benzimidazol-1-ylmethyl)phenyl]methyl]−4-bromo-1*H*-pyrrole-2-carboxamide (BL5) as a highly potent and selective hIDO1 inhibitor discovered by our group, that was initially described as a classical catalytic inhibitor (A375, IC_{50} = 16 nM; compound 10 of the following reference [23]), but turned out to act as an apo-inhibitor according to diverse biophysical, enzyme and cell-based assays (data not shown). The chemical structures of all studied hIDO1 inhibitors together with that of a selective TDO inhibitor (680C91) are depicted in Fig. 2.

2. Materials and methods

2.1. Reagents

Tryptophan (TRP), L-kynurenine (KYN), xanthurenic acid (XA), 3-hydroxykynurenine (3OHKYN), kynurenic acid (KA), 3-hydroxyanthranilic acid (3OHAA), anthranilic acid (AA), 5-hydroxytryptamine (serotonin, 5HT), tryptamine (TRYP), and L-tryptophan-(indole-d_5) (d_5T - internal standard, IS) were supplied from Sigma-Aldrich (Cat. Nos. T2610000, K8625, D120804, H1771, K3375, 148776, A89855, 14927, 193747, and 615862). Dimethyl sulfoxide (DMSO) and trichloroacetic acid (TCA) were also purchased from Sigma-Aldrich (Cat. Nos 34869–1 L and T6399). LC-MS grade formic acid (FA), methanol (MeOH) and water were purchased from Carlo Erba (Milan, Italy, Cat. 414831 and 412111). EP was purchased from Selleck Chemicals GmbH (Planegg, Germany, Cat. No. S7910). LIN was supplied from D.B.A. ITALIA S.R.L. (Cat. No. 1923833–60–6). BL5 compound was synthesized in-house according to the procedure available in the following reference. [23] 680C91, a selective hTDO inhibitor, was purchased from Sigma-Aldrich (Cat. No SML0287). Dulbecco's Modified Eagle's Medium (DMEM) and Eagle's Minimum Essential Medium (EMEM) were obtained from Sigma Aldrich (Milan, Italy) fetal bovine serum (FBS), L-glutamine, penicillin and streptomycin were obtained from Immunological Sciences (Rome, Italy).

2.2. Preparation of standard solutions

The stock solutions (SSs) were prepared as follows: i) preparation of 5 g/L DMSO solution for each analyte; ii) 1:50 dilution and mixing of all compounds with DMSO to reach 1.0×10^5 μg/L concentration; iii) partition of the multiplex analyte solution in 1.5 mL microcentrifuge tubes; iv) 1:5 dilution with H_2O or matrix to get a working solution (WS) at 20,000 μg/L. v) Calibrators and quality controls (QCs) solutions were prepared by further water-diluting the WS. A group of seven calibrators were prepared to cover a range of concentrations from 5 to 200 μg/L (5HT, TRYP, XA, KA and AA), 200 or 500–20,000 μg/L (3OHKYN, KYN, 3OHAA and TRP) by serial dilutions. For the first range the QCs were

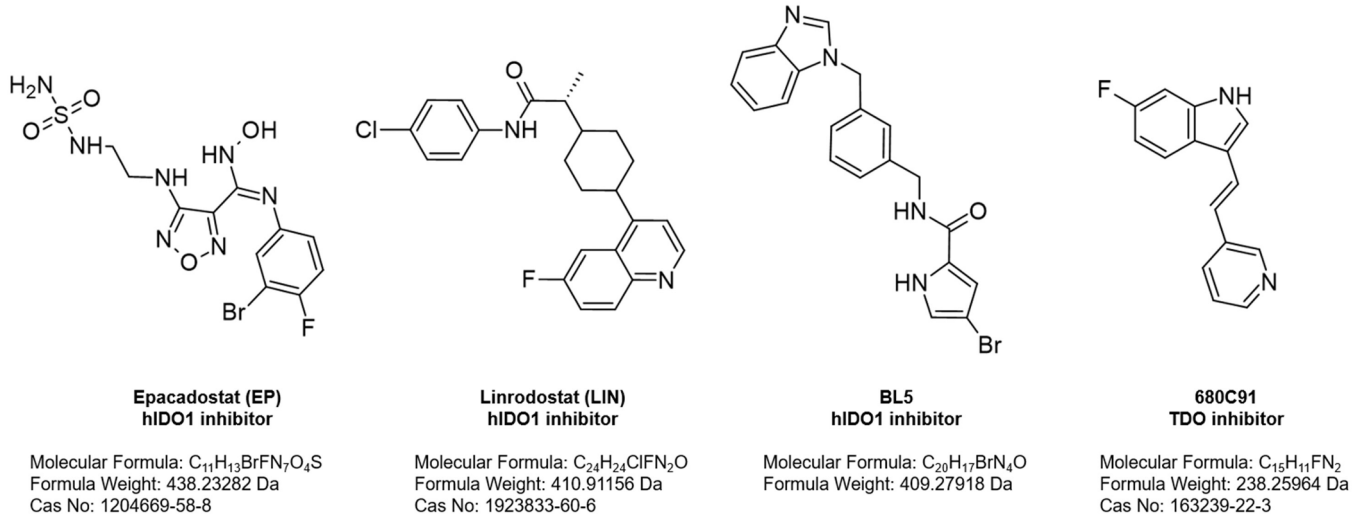

Fig. 2. Chemical structures of hIDO1/TDO selective inhibitors.

5 μg/L (Lower Limit of Quantification - LLOQ), 7.5 μg/L (Low QC - LQC), 75 μg/L (Medium QC - MQC) and 150 μg/L (High QC - HQC). Similarly for the second, which included 200 or 500 μg/L (LLOQ), 500 or 750 μg/L (LQC), 7,500 μg/L (MQC) and 15,000 μg/L (HQC).

IS stock and its diluted solutions (IS solution) were prepared as follows: IS stock 5 g/L solution was progressively watered-down up to 500 μg/L for d_5T and then diluted 1:10 in a mixture of H_2O:MeOH:TCA 10% (*w/v*) 40:15:45 *v/v/v* to the final concentration of 50 (IS solution). The IS solution was used for matrix protein precipitation during sample preparation. Blank and zero samples were prepared using the cell culture media matrices (DMEM, EMEM) as the basis. Standard solutions (calibrators, QCs, blank and zero samples) were prepared daily.

2.3. Sample preparation

Standard and study samples were treated as follows: 40 μL aliquots of each sample were collected in a microcentrifuge tube after addition of 400 μL of IS solution (d_5T 50 μg/L). The diluted samples were vortexed for 1 min and centrifuged at 13,000 rpm for 5 min. 400 μL aliquots of each supernatant were analyzed by LC-MS/MS. Analogously, standard matrix-matched samples were obtained by spiking the matrix with the calibrator or QC solutions, as follows: 40 μL aliquots of the calibrator or QC solution were combined with 40 μL of the matrix, followed by the addition of 400 μL of the internal standard (IS) solution. This resulted in the creation of equally 10-fold diluted matrix-matched samples. Standard samples were then used to construct either an external calibration curve or a matrix-matched curve, which was essential for assessing the matrix effect. This involved constructing an external calibration curve or a matrix-matched curve to assess the matrix effect.

Blank samples were prepared using the same procedure, excluding the addition of IS solution. Instead, an equivalent amount of free-IS solution was added, prepared according to the description in paragraph 2.2.

2.4. Instrumentation and chromatographic conditions

2.4.1. LC-MS/MS analyses

A Q-Exactive Plus UHMR Hybrid Quadrupole Orbitrap™ Mass Spectrometer equipped with a Vanquish™ Duo UHPLC system was employed (Waltham, MA, USA). The chromatography equipment included a Synergi 4 μm Polar-RP 80 Å, LC 150 × 2 mm column protected by a Polar-RP SecurityGuard cartridge (4 × 2.0 mm - Phenomenex, Torrance, CA, USA) maintained at 45 °C, and the mobile phase composed of H_2O 0.1% *v/v* FA (solvent A) and MeOH 0.1% *v/v* FA (solvent B) at the flow rate of 0.300 mL/min. The gradient elution progresses through a series of steps defined by the proportions of solvent A and B, as follows: 5%− 80% solvent B in 5 min, up to 95% solvent B from 5.0 to 8.0 min, held at 95% solvent B for 1.0 min, then column reconditioning at 5% solvent B from 9.0 to 14.0 min. The injection volume was 5 μL. Electrospray Positive ionization mode (ESI^+) was set with the following operating conditions: spray voltage, 3.50 kV; capillary temperature, 350 °C; sheath gas flow (N_2) 45.00 L/min; sweep gas (N_2) flow 0.00 L/min; Aux gas (N_2) flow rate 30.00 L/min heated to 350 °C, Max Spray Current 100.00 μA. MS detection data were collected in parallel reaction monitoring (PRM). MS conditions and transitions of each analyte under collision energy conditions ranging from 10 to 35 eV are summarized in Table 1. In most cases, PRM fragmentation yielded multiple ion transitions, as follows per each analyte: 5HT (177.102 m/z > 160.076,134.956 m/z), TRP (205.097 m/z > 188.071, 146.060 m/z), KYN (209.092 m/z > 192.066, 94.065 m/z), 3OHKYN (225.087 m/z > 208.060, 110.060 m/z), *and* d_5T *(*210.129 m/z > 192.096,150.029 m/z*).* Single product ions were registered for AA (138.055 m/z > 120.444 m/z), 3OHAA (151.050 m/z > 136.039 m/z), XA (206.045 m/z > 178.049 m/z), KA (190.050 m/z > 162.055 m/z) and TRYP (161.107 m/z > 144.081 m/z). We subsequently selected the most abundant transitions with minimal background noise for quantification (Supporting Information, Fig. 1S). For almost all of the analytes, including AA, 3OHAA, TRYP, 5HT, TRP, KYN, 3OHKYN, and d5T, the

Table 1
PRM database records for kynurenines. Chromatograms are reported in Fig. 3. MS spectra were acquired and processed using Xcalibur® software (Thermo Fisher Scientific).

Analyte	MW [g/mol]	Ion mode	MS1 [m/z]	MS2 [m/z]	Collision Energy [eV]
AA	137.1360	ESI^+	138.055	120.444	15
3OHAA	153.1354	ESI^+	154.050	136.039	15
TRYP	160.2157	ESI^+	161.107	144.081	35
5HT	176.2151	ESI^+	177.102	160.076	20
				134.956	
KA	189.1675	ESI^+	190.050	162.055	10
TRP	204.2252	ESI^+	205.097	188.071	10
				146.060	
XA	205.1669	ESI^+	206.045	178.049	10
KYN	208.2139	ESI^+	209.092	192.066	10
				94.065	
3OHKYN	224.2133	ESI^+	225.087	208.060	10
				110.060	
d_5T	209.2560	ESI^+	210.129	192.096	10
				150.029	

best transition was the product ion at − 18 *m/z*, which is consistent with the loss of a water molecule from the corresponding precursor ion.

2.4.2. LC-MS/MS method validation

The method was validated according to the bioanalytical method validation guidelines provided by FDA, EMA, and ICH M10 guideline draft version. [24–26] The method compliance was tested in terms of linearity, accuracy, precision, recovery, selectivity, matrix effect, carry-over and stability. Specifically, we optimized and validated the current method based on our earlier LC-MS/MS procedure. [27,28]

2.4.2.1. Linearity. The calibration curves were plotted over seven concentration levels ranging from 5 μg/L to 20,000 μg/L, in the presence of the IS. Method validation experiments were conducted over three independent runs by using freshly prepared standard solutions as described in paragraphs 2.2 and 2.3. The instrument response was calculated as the ratio between the analyte and IS area after integration by Xcalibur® software. The relationship between analyte/IS peak area ratios and analyte concentration were graphed by using 1/x weighted linear regression.

2.4.2.2. Accuracy and precision. Within-run accuracy (AC) and precision were assessed for each QC level by analyzing five different subsamples, all derived from the extraction of the same QC solution. For between-run validation, each QC level was evaluated in three runs over three different days.

2.4.2.3. Matrix effect. The matrix effect was evaluated by comparing the response of the analyte after addition of the matrix with the response of the analyte in neat solvent at low, medium and high concentrations. Each level was analyzed in triplicate. Moreover, the matrix effect was assessed also through the slope-ratio of a 10-fold diluted matrix-matched curve against the curve in neat solvent, multiplied by 100. [29–31]

2.4.2.4. Stability assays and carry-over. Freeze-thaw and autosampler stabilities were assayed by analyzing low, medium and high QC in triplicate. Freeze-thaw stability assay was carried out over three freeze-thaw cycles from − 80 °C to room temperature. The procedure began with non-extracted samples, followed by the treatment of a single aliquot as detailed in paragraph 2.3 after each freeze-thaw cycle (interval of 24 h). The stability of the autosampler was assessed by analyzing quality control (QC) samples that had been stored at 15 °C for 24 h. For this assessment, previously extracted samples were used and analyzed within the specified time frame. Throughout the entire validation period, potential carry-over effects were continuously monitored by analyzing solvent blanks (H_2O:MeOH 50:50, *v/v*) after reaching the Upper Limit of Quantification (ULOQ) in order to exclude any potential memory effect along the analytical sequence.

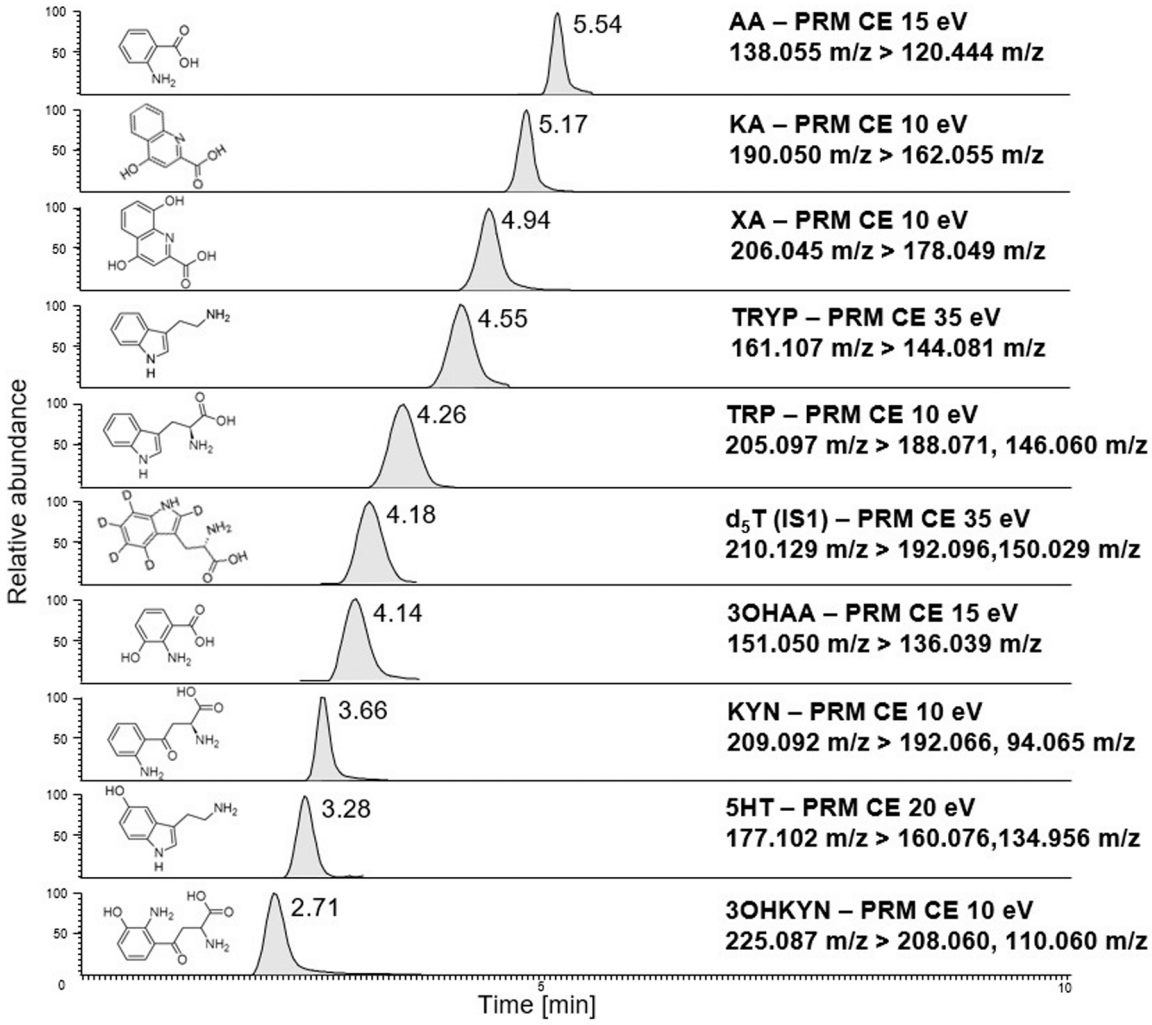

Fig. 3. Mass chromatograms of the analytes. Chromatography peaks of KYNs and ISs in neat solvent spiked with 7500 μg/L of each analyte obtained by isolating the corresponding most specific product ions (*m/z* on the right) in descending order of retention time from the top to the bottom.

2.4.2.5. Specificity. The method's specificity was evaluated analyzing the blank matrices (DMEM, EMEM), known for their industrial reproducibility, as well as matrices spiked with standard solutions at LLOQ levels and IS (IS solution). According to the ICH guideline M10, responses due to interfering components should not exceed the 20% of the analyte response at the LLOQ, and not more than 5% of the IS response.

2.5. Cell lines

U87 (glioblastoma cell line, Cellosaurus RRID: CVCL_0022) and MDA-MB-231 (Breast cancer cell line, Cellosaurus RRID: CVCL_0062), were kindly provided by Prof Armando Genazzani (Department of Pharmaceutical Sciences, University of Piemonte Orientale, Novara Italy); A375 (Melanoma cell line, Cellosaurus RRID: CVCL_0132) was offered by Prof. Giuseppina Comito (Department of Experimental and Clinical Biomedical Sciences, Biochemistry, Human Health Medical School, University of Florence, Florence Italy).

MDA-MB-231 and A375 cell lines were cultured in high glucose DMEM (Sigma-Aldrich) supplemented with 10% of heat inactivate fetal bovine serum (FBS), 2 mM L-glutamine, 100 IU/mL penicillin and 100 μg/mL streptomycin (Immunological Sciences) and kept in a 37 °C incubator with 5% CO_2. While, U87 cells were cultured in EMEM (Sigma-Aldrich) supplemented with 10% FBS 2 mM L-glutamine, 100 IU/mL penicillin and 100 μg/mL streptomycin (Immunological Sciences) and kept in a 37 °C incubator with 5% CO_2.

2.6. Media preparation and cell treatments

Cell culture media were selected according to the different cell types and were freshly prepared immediately prior to use. In a total volume of 100 mL of medium, 2,000 U/mL of interferon γ (IFNγ) and IDO1 inhibitor were added at different concentration ranges (0.2–600 nM, 0.02–20,000 nM and 2–20,000 nM for LIN, BL5 and EP, respectively). U87 cells were also treated with TDO inhibitor SML0287 at 10 and 30 μM.

2.7. Media preparation and cell treatments

RNA extraction and RT-PCR analysis were performed as previously described. [32] Briefly, A375 and was cultured in presence absence of 1000 U/mL IFNγ for 48 h, harvested, and centrifuged at 1000 × *g* for 5 min at 4 °C. Total RNA was isolated using the GenElute™ mammalian total RNA miniprep kit (Sigma-Aldrich) and reverse-transcribed using the ThermoScript™ RT–PCR kit (Life Technologies) according to the manufacturer's instructions. For amplification, 3 μL of cDNA was added to GoTaq FlexiDNA Polymerase in 25 μL reaction buffer, containing 0.5 mM of forward and reverse primers (Supporting Information, Table 1S). RT-PCR amplicons were resolved in a 1% agarose gel by electrophoresis, and signals were quantified with densitometric analysis software (NIH Image 1.32; National Institutes of Health, Bethesda, MD, USA).

2.8. Applications

2.8.1. Cell experiments and treatments

A375, MDA-MB-231 and U87 cell lines were pleated 5,000 cells/well in 100 μL of specific medium in a 96 MW and left to adhere overnight in a 37 °C incubator with 5% CO_2. The day after the media of treatment were added to the cell obtaining the concentration required for each inhibitor (0.1–300 nM, 0.01–10,000 nM and 1–10,000 nM for LIN, BL5 and EP, respectively). After 48 h of incubation at 37 °C with 5% CO_2, plates were centrifuged 5 min at 1,200 rpm, supernatants collected and stored at − 80 °C until use, namely sample dilution followed by LC-MS/MS analysis.

2.8.2. Determination of half maximal inhibitory concentration and data analysis

The half maximal inhibitory concentration (IC_{50}) is a remarkable pharmacological parameter in preclinical drug development, which measures the potency of an inhibitor against a specific biological or biochemical function. The IC_{50} of known molecules were determined to compare the obtained results with data already published in the literature. The experiments were conducted in quadruplicate (n = 4).

The concentrations that caused a 50% inhibition of hIDO1 activity (IC_{50}) were determined from the dose-response curves using the "log (inhibitor) *vs.* normalized response" function of GraphPad software (GraphPad Prism 9.1.0). The x-axis represents the concentration of the inhibitor (in nM), while the y-axis represents the activity percentage of hIDO1 expressed as the KYN/TRP ratio. The y-values were normalized by setting both the maximal and basal controls (100% and 0% CTRLs), which correspond to the IFNγ-treatment and the basal conditions, respectively. For each tested inhibitor three different values of $IC_{50} \pm SE$ were determined, one for each of the three selected cell lines (Fig. 4).

The goodness of fit of the statistical models used to describe the dose-response curves was evaluated in terms of r^2 (coefficient of determination) and Sy.x (Standard Error of Estimate). All dose-response curves were superimposed based on the cell line and tested inhibitor to assess differences in terms of efficacy and potency.

The concentration data of the tryptophan catabolites obtained from our targeted-metabolomic approach were processed using Metaboanalyst 5.0. The data were sorted based on experimental conditions, specifically the basal condition (positive control) with no hIDO1 induction, IFN (negative control) with fully-operative hIDO1, and the inhibitors categorized by their mechanism of action. The inhibitors included iAPO (hIDO1 apo inhibitors: LIN, BL5), iHOLO (hIDO1 holo inhibitor: EP), and iTDO (TDO inhibitor: 680C91). All the inhibitors considered in this step have been used at twice their corresponding IC_{50} value to formally represent a 100% inhibition of the enzyme.

All the data were normalized using cube root transformation to achieve a normal distribution of the dataset. The subsequent statistical analysis involved PCA (principal component analysis) to identify 95% confidence interval areas, biplot analysis to visualize variable changes across samples, correlation analysis among the analytes, and heatmaps depicting the clusterization of metabolic data using Ward's method.

To evaluate the modulation of KYN/TRP ratio given by the selective TDO inhibitor (680C91) in the A375, MDA-MB-231, and U87 cell lines, GraphPad Prism software was employed. All data were normalized by setting both the maximal and minimal values as 100% and 0% both in the basal and IFNγ induction conditions. To identify statistically significant differences in KYN/TRP ratio between the groups, the normalized data underwent two-way ANOVA followed by Tukey's multiple comparison test (* $p < 0.05$; ** $p < 0.01$; *** $p < 0.001$; **** $p < 0.0001$).

3. Results and discussion

3.1. Development and optimization of LC-MS/MS conditions and sample preparation

Kynurenines are chemical entities characterized by diverse chemical-physical properties, which influence their chromatographic separation and MS detection. Among these properties, water solubility and acidity/basicity play a crucial role. 3OHKYN suffers from a well-known aqueous instability caused by the 2-amino-3-hydroxyphenyl substitution, which is susceptible to spontaneous oxidation, forming the corresponding iminoquinone derivative. The aqueous degradation of 3OHKYN occurs gradually, flanked by color changing yellow-brown. For this reason, aqueous solutions should not be stored for more than 24 h, as also suggested by the technical label and reported in literature. [14] From a validation point of view, a mixed solution containing all analytes at known concentrations is more feasible, even though this is not always

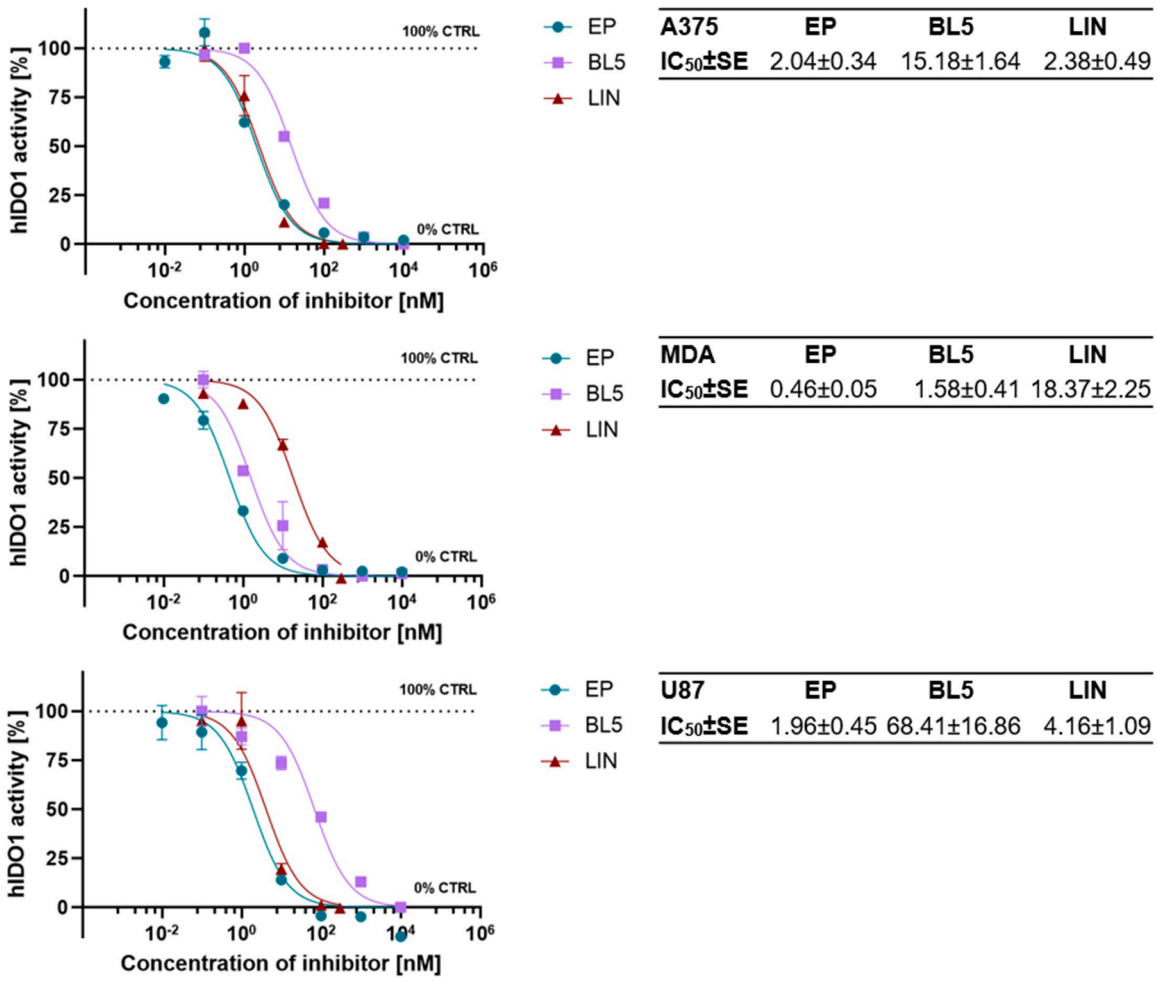

Fig. 4. Dose-response curves of the tested hIDO1 inhibitors. The x-axes represent the logarithm base 10 of the inhibitor concentrations displayed as power of 10 (nM), whereas the y-axes hIDO1 activity percentage, expressed as KYN/TRP ratio. The error bars display the Standard Errors of the Mean (SEM). The vertical dotted lines indicate the IC_{50} in each experimental condition, which is reported above every single graph (cell line - tested compound).

possible due to solubility issues. Hence, in this paper SSs were prepared using DMSO to freshly solubilize all KNSs of interest at 1 mg/mL w/v, followed by serial dilutions with H_2O or matrix to make calibrators and/or QCs. Furthermore, organic solvents degrade 3OHKYN through a slower kinetics, confirmed by the fact that no variation was observed during the validation time-lapse.

During the method optimization, solvents and dilutions were tested to maximize the protein precipitation, plus the chromatography quality, and efficiency. Pure acetonitrile (ACN) and methanol were quickly excluded from the sample preparation, due to LC peak splitting, which occurs for kynurenines, such as KYN, mostly at concentrations $\geq$ 500 μg/L, hypothetically caused by the pH conditions. We dealt with this issue by acidifying the organic modifier, *de facto* methanol gave a better separation than ACN, which was further improved after the addition of organic acids, mostly TCA. Nevertheless, TCA is an acclaimed ESI ionization suppressor. Thus, we found a compromise in terms of peak shape and MS signals by introducing 10% *w/v* TCA only in sample pretreatment, and 0.1% *v/v* FA as eluent additive (paragraphs 2.3 and 2.4.1).

Concerning the chromatography, kynurenines are not efficiently retained by C18 reverse phase columns, since they tend to elute close to the hold-up time, as detailed in our previous paper on kynurenines. [23,27,28] Herein, we selected a Synergi 4 μm Polar-RP 80 Å (150 ×2 mm), which is functionalized with phenyl ether groups and polar endcapping, that promote the retention of polar and aromatic analytes selectively. The chromatography tuning involved the elution optimization by regulating the gradient composition to get better peak resolution and a rational run-time. The LC conditions, reported in the paragraph 2.4.1, enabled an excellent separation of the kynurenines in the first 7 min of analysis, subsequently followed by column reconditioning for a total run time of only 14 min (Fig. 3).

The MS detection of the kynurenines was carried out by targeted metabolomics using the PRM mode, which acquired MS^2 scans based on the inclusion list reported in Table 1. PRM mode is widely used for the quantification of small molecules present in complex matrices to get a high grade of selectivity. Hence, this methodology is particularly suited to our future purposes of quantifying KP metabolites in plasma and other biological fluids.

d_5T, a deuterium (D)-labeled derivative of TRP bearing 5 D atoms incorporated into the indole moiety, was selected as internal standard (IS) due to its close correlation with natural kynurenines and high detectability by LC-MS/MS.

3.1.1. Validation and chromatography/mass spectrometry analyses

Here, we propose a qLC-HRMS method for the assessment of the KP in two different cell culture media: DMEM (Dulbecco's Modified Eagle Medium) and EMEM (Essential Modified Eagle's Medium). Linear relationships between the nominal concentration of analytes and their instrumental response were confirmed in both matrices from 5 to 20,000 μg/L. As shown in Table 2, calibration curves have a determination coefficient (r^2) > 0.99 and intercept nearly to zero or origin, in addition to wide working ranges of calibration per each analyte.

Table 2
Linearity parameters of kynurenines. List of linearity ranges, r^2, LLOQ, and LLOD for each analyte.

Analyte	Linearity range [μg/L]	r^2	LLOQ [μg/L]	LLOD [μg/L]	
AA	5–200	0.9954	5	0.6*	0.4§
3OHAA	500–20,000	0.9958	500	389.6*	363.3§
TRYP	5–200	0.9949	5	2.9*	0.5§
5HT	5–200	0.9944	5	1.4*	2.4§
KA	5–200	0.9949	5	3.1*	2.4§
TRP	500–20,000	0.9973	500	-	-
XA	5–200	0.9975	5	0.1*	1.1§
KYN	200–20,000	0.9981	200	162.6*	188.2§
3OHKYN	500–20,000	0.9948	500	155.5*	95.5§

* DMEM matrix, § EMEM matrix

As shown in Tables 3–4, precision, accuracy (AC), matrix effect (ME) and stability data complied with bioanalytical validation requirements: i) intra and inter-day precisions (%RSDs) respect the range ± 15% of nominal concentrations ii) intra and between-run accuracies respected the acceptance criteria established by FDA guidelines, since they ranged from 1.0% to 10.1%. Negligible interferences lower than 20% of the analyte response were detected at the corresponding LLOQ level, which confirm the method's specificity (Supporting Information, Figs. 2S, 3S).

Regarding TRP, the LLOD calculation was not feasible due to its high concentration in the cell culture media. This outcome was predictable since we have not adopted activated charcoal to remove the TRP from the cell culture media as other published methods. [14,22] The calibration function led to quantifying the content of TRP in the cell culture media giving values equivalent to the medium labeled concentrations. Furthermore, TRP content is merely reproducible in the quantification range of interest, in which we demonstrated that the matrix curves and the calibration function in solvent share the same slope (Supporting Information, Fig. 4S).

In this work, cell culture media with a specific and reproducible composition were employed as matrices, where interferences were negligible and MS detection provided with an excellent specificity (Supporting Information, Fig. 2S-3S).

Of note, the analyzed matrices did not produce any significant changes in terms of instrumental response. The slope-ratio MEs ranged from 90% to 110%, as obtained by comparing the response at the QC levels. To make a comparison with the solvent curve, the matrix-calibration curves of TRP were corrected by subtracting the concentration of TRP included in DMEM and EMEM blanks.

Surprisingly, when comparing the slopes, the matrix effect consistently falls within the acceptance range, indicating a low matrix effect in both DMEM and EMEM. It is worth noting that there are no validated methods reported in the literature for assessing the matrix effect in EMEM, unlike our study. The disparity between DMEM and EMEM can be attributed to the discrepancy in amino acid and vitamin concentrations, with DMEM containing four times higher levels, as stated on the label. To visualize this difference, please refer to the matrix-matched curve provided in the Supporting Information (refer to Supporting Information, Fig. 4S).

As detailed in Table 4, most of the kynurenines were stable after three freeze-thaw cycles and 24 h at 15 °C. However, the response of

Table 3
Validation parameters in DMEM and EMEM matrices. For each analyte, Intra (INDP) and InTer-Day Precisions (INDP, ITDP) expressed as %RSD, Accuracy (expressed as average of absolute values) Within and Between-Run (WRA, and BRA), Matrix Effects (MEs) are reported.

Analyte	QC level	INDP (%RSD, n = 5)	ITDP (%RSD, n = 11)	WRA (n = 5)	BRA (n = 11)	ME (%) $_{\text{slope ratio}}$		ME (%)	
AA	LLOQ	3.5	13.6	9.8	12.7	93.2*	97.4§	102.3*	105.8§
	LQC	0.4	8.7	1.3	5.9			99.4*	99.6§
	MQC	6.4	7.8	5.8	6.2			108.1*	107.5§
	HQC	3.3	5.7	3.1	4.7			103.6*	101.2§
3OHAA	LLOQ	8.3	5.8	19.8	18.8	98.1*	96.1§	98.7*	106.4§
	LQC	2.6	3.6	8.6	7.0			78.6*	83.9§
	MQC	0.6	1.8	1.9	2.7			98.8*	95.1§
	HQC	2.8	4.7	2.8	4.1			101.0*	97.7§
TRYP	LLOQ	5.6	14.8	15.8	14.0	108.3*	108.0§	97.2*	100.5§
	LQC	2.2	9.6	6.8	7.7			102.1*	103.8§
	MQC	3.5	3.6	2.9	2.8			101.7*	98.9§
	HQC	1.3	3.3	1.0	2.6			99.0*	91.0§
5HT	LLOQ	0.5	6.4	2.8	6.0	101.4*	105.1§	101.9*	99.6§
	LQC	0.4	10.5	10.1	9.3			95.3*	96.7§
	MQC	2.9	8.1	4.9	6.7			99.9*	101.7§
	HQC	8.7	8.3	9.3	7.2			97.3*	103.0§
KA	LLOQ	11.0	12.5	16.8	10.6	105.1*	104.4§	109.1*	108.5§
	LQC	5.3	7.4	7.7	7.5			112.8*	114.6§
	MQC	8.8	6.3	6.7	5.5			96.2*	100.9§
	HQC	3.6	6.7	6.7	6.1			97.0*	100.6§
TRP	LLOQ	4.4	6.8	12.8	12.1	105.5*	105.3§	108.5*	101.9§
	LQC	1.6	2.4	6.6	5.4			99.6*	99.9§
	MQC	2.6	3.6	2.0	2.8			101.8*	101.6§
	HQC	0.3	4.5	1.7	3.2			99.4*	99.7§
XA	LLOQ	8.1	17.7	12.2	14.3	101.2*	100.4§	96.4*	103.7§
	LQC	4.9	9.6	5.3	7.3			102.0*	96.5§
	MQC	7.9	8.0	6.4	6.8			97.3*	97.3§
	HQC	3.0	4.2	2.1	2.9			99.9*	99.8§
KYN	LLOQ	3.0	7.1	14.7	8.9	97.0*	98.3§	104.6*	107.9§
	LQC	4.2	4.5	2.7	3.4			106.5*	113.6§
	MQC	1.9	2.7	2.1	2.4			105.0*	101.8§
	HQC	2.1	3.5	3.2	2.9			103.1*	117.7§
3OHKYN	LLOQ	7.4	2.6	13.4	16.1	101.9*	98.6§	98.1*	91.8§
	LQC	2.9	3.1	2.2	2.6			88.6*	91.2§
	MQC	2.8	2.4	3.7	4.1			99.9*	94.2§
	HQC	7.1	4.7	6.4	4.7			97.4*	98.1§

* DMEM matrix, § EMEM matrix

Table 4
Stability data of the operating conditions. For each analyte, freeze-thaw cycle (−80 °C to room temperature), autosampler (15 °C for 24 h), and Bench-top (room temperature ~20 °C for 12 h) stabilities are reported.

Analyte	QC level	Freeze-thaw stability, I-III cycles (n = 9)		Autosampler stability 15 °C, 24 h (%RSD, n = 6)	Bench-top stability 20 °C, 12 h (%RSD, n = 3)
AA	LQC	11.5*	8.3§	4.0	6.2
	MQC	-6.6*	13.4§	6.5	13.1
	HQC	6.3*	9.8§	6.0	8.0
3OHAA	LQC	-20.9*	-20.8§	3.7	5.3
	MQC	-32.1*	-33.2§	1.5	8.1
	HQC	-33.6*	-15.4§	5.7	3.9
TRYP	LQC	5.4*	11.3§	8.7	4.1
	MQC	14.1*	-9.4§	4.3	2.1
	HQC	10.9*	14.2§	4.4	2.4
5HT	LQC	8.3*	13.7§	14.5	13.9
	MQC	-10.1*	-1.6§	12.4	11.8
	HQC	15.0*	12.5§	13.8	5.5
KA	LQC	-0.8*	10.9§	7.8	5.0
	MQC	-3.0*	-2.4§	3.8	5.7
	HQC	-10.2*	-8.9§	7.0	1.9
TRP	LQC	-1.2*	-10.8§	2.1	3.4
	MQC	-9.6*	-13.7§	8.2	7.7
	HQC	-13.1*	1.3§	9.2	3.0
XA	LQC	14.2*	8.1§	5.1	9.1
	MQC	-6.3*	-1.2§	7.8	5.1
	HQC	-14.4*	-11.6§	4.9	4.5
KYN	LQC	-0.7*	14.4§	4.3	3.3
	MQC	2.9*	0.4§	3.2	1.3
	HQC	-4.8*	9.6§	2.6	1.2
3OHKYN	LQC	-3.7*	-9.5§	6.3	3.2
	MQC	-33.2*	-32.9§	2.4	5.3
	HQC	-38.1*	-15.7§	2.3	1.1

* DMEM matrix, § EMEM matrix

3OHAA and 3OHKYN are outside the ± 15% acceptance range also after a single freeze-thaw cycle (≈−30%), suggesting the need to analyze these metabolites daily immediately after sampling.

3.2. Cell-based hIDO1 inhibition assay via LC-MS/MS

The developed LC-MS/MS method for quantification of KP catabolites in cell cultures was applied to estimate the IC_{50} value of EP, LIN, and BL5 in three distinct cancer cell lines (A375, MDA-MB-231, and U87). Importantly, our method considered the changes in the levels of both kynurenine (KYN) and tryptophan (TRP) as KYN/TRP ratio. This comprehensive approach provides a more comprehensive understanding of the compound's efficacy and potential implications in the context of the kynurenine pathway.

The proposed LC-MS/MS method for quantification of KP catabolites in cell cultures led to estimating the IC_{50} value of EP, LIN and BL5 in three different cancer cell lines (A375, MDA-MB-231 and U87) considering the changes in the level of both KYN and TRP, on the contrary of other studies which only consider KYN. Interestingly, the holo inhibitor EP showed higher inhibitory potency than both apo-inhibitors BL5 and LIN in all experimental conditions tested, with IC_{50} values of 2.04 ± 0.34 nM in A375, 0.46 ± 0.05 nM in MDA-MB-231 and 1.96 ± 0.45 nM in U87 cell lines. This phenomenon could be associated with the fact that hIDO1 exists in an equilibrium between holo- and apo-form, which, in turn, depends on both cellular levels of hIDO1 and heme. On the other hand, all tested compounds shared a similar *in vitro* efficacy, given that they similarly lowered the levels of kynurenine in the extracellular space considering the overlap of the curve trends at the background effect (the plateau observed for large drug concentrations).

While no significant differences of activity were observed for EP in the tested cell lines, LIN showed lower potency in MDA-MB-231 cells (IC_{50} = 18.37 ± 2.25 nM) compared to A375 and U87 cells (IC_{50} = 2.38 ± 0.49 and 4.16 ± 1.09 nM, respectively) and BL5 displayed higher potency in MDA-MB-231 cells (IC_{50} = 1.58 ± 0.41 nM) than in A375 and U87 (IC_{50} = 15.18 ± 1.64 and 68.41 ± 16.86 nM, respectively). The obtained results are in line with the literature. [23] Further investigations are required to understand if the poor correlation among IC_{50} values in the three cell lines depends on differences in either heme synthesis or other cellular specific phenomena.

In light of these results, the proposed LC-MS/MS cell-based assay allowed a reliable estimation of the IC_{50} values for all tested inhibitors, thereby representing a screening method for identifying and characterizing new hIDO1 inhibitors.

3.3. Multivariate analysis and comparative study

The developed LC-MS/MS method enabled the quantification of kynurenine in A375, MDA-MB-231, and U87 cell lines, both in the presence (NC: negative control) and absence of IFNγ stimulation (PC: positive control). The main kynurenines were tracked to investigate the effect of selective inhibition of hIDO1 by EP, LIN, and BL5, as well as the selective inhibition of TDO by 680C91. Statistical analysis based on the quantified concentrations of analytes (XA, KA, AA, KYN, and TRP) in different experimental conditions was performed using the Metaboanalyst 5.0 web platform, as depicted in Figs. 5, 6, and 7. PCA allows for the explanation of variance in a dataset (X) without referring to class labels (Y). The distribution of each group provides information about the correlation between diverse experimental conditions.

As illustrated in Figs. 5A, 6A, and 7A, the IFN groups and the treatments with 680C91 (iTDO) are closely located mostly in the A375 cell line, suggesting no significant inhibition or expression of TDO (Fig. 5A). However, in the MDA-MB-231 and U87 cell lines (Figs. 6A, 7A), which are known to express TDO according to literature references, 33,34 there is a different distribution between IFNγ and iTDO, highlighting the inhibition of TDO. This distinct metabolic signature, in comparison to hIDO1 inhibition, suggests that TDO plays a marginal but not negligible role in the production of kynurenines. Heat maps are provided in the Supporting Information, specifically Fig. 5S. The delineation of the 95% confidence interval (CI) in PDA facilitated an initial clusterization of the experimental groups based on the quantified metabolites, which was further verified through Hierarchical Clustering analysis (see Supporting Information, Fig. 6S). The integration of dendrograms and heatmaps yielded significant insights into the interconnections and patterns among the samples.

Interestingly, in all cell lines, the feature of IFN against iTDO entered the same main group and then separated into subgroups, although the separation is not pronounced in the A375 cell line due to partial overlap between IFN and iTDO. Conversely, the features related to the mechanism of action (iAPO, iHOLO) suggest that they may affect TRP metabolism differently. However, this finding cannot be confirmed in the MDA-MB-231 cell line, where there is partial superimposition between iAPO and iHOLO. In general, additional investigations are warranted to delve deeper into the matter.

PCA enables the exploration of how variables change within the dataset through biplots (Figs. 5B, 6B, and 7B). In particular, the vectors indicate higher concentrations of TRP in samples treated with hIDO1 inhibitors, while IFN and iTDO conditions exhibit elevated levels of KYN and other downstream metabolites, indicating that metabolism is enhanced by IFNγ induction, which is only partially inhibited by 680C91 in MDA-MB-231 and U87 cell lines. The heat maps also highlight this 'seesaw' effect, where subsequent hIDO1 inhibition increases TRP levels by blocking the formation of downstream catabolites (Figs. 5C, 6C, and 7C). In other words, IFNγ stimulation promotes kynurenine synthesis, with TRP acting as a trigger. The levels of TRP are higher in the PC due to the absence of hIDO1 expression. An expected decrease in TRP concentrations was observed in each cell line after IFNγ stimulation, while KYN levels increased significantly, leading to an increase in downstream enzymes of the KP pathway and subsequently higher levels of KA, AA, and XA. In the presence of hIDO1 inhibitors, the levels of kynurenines

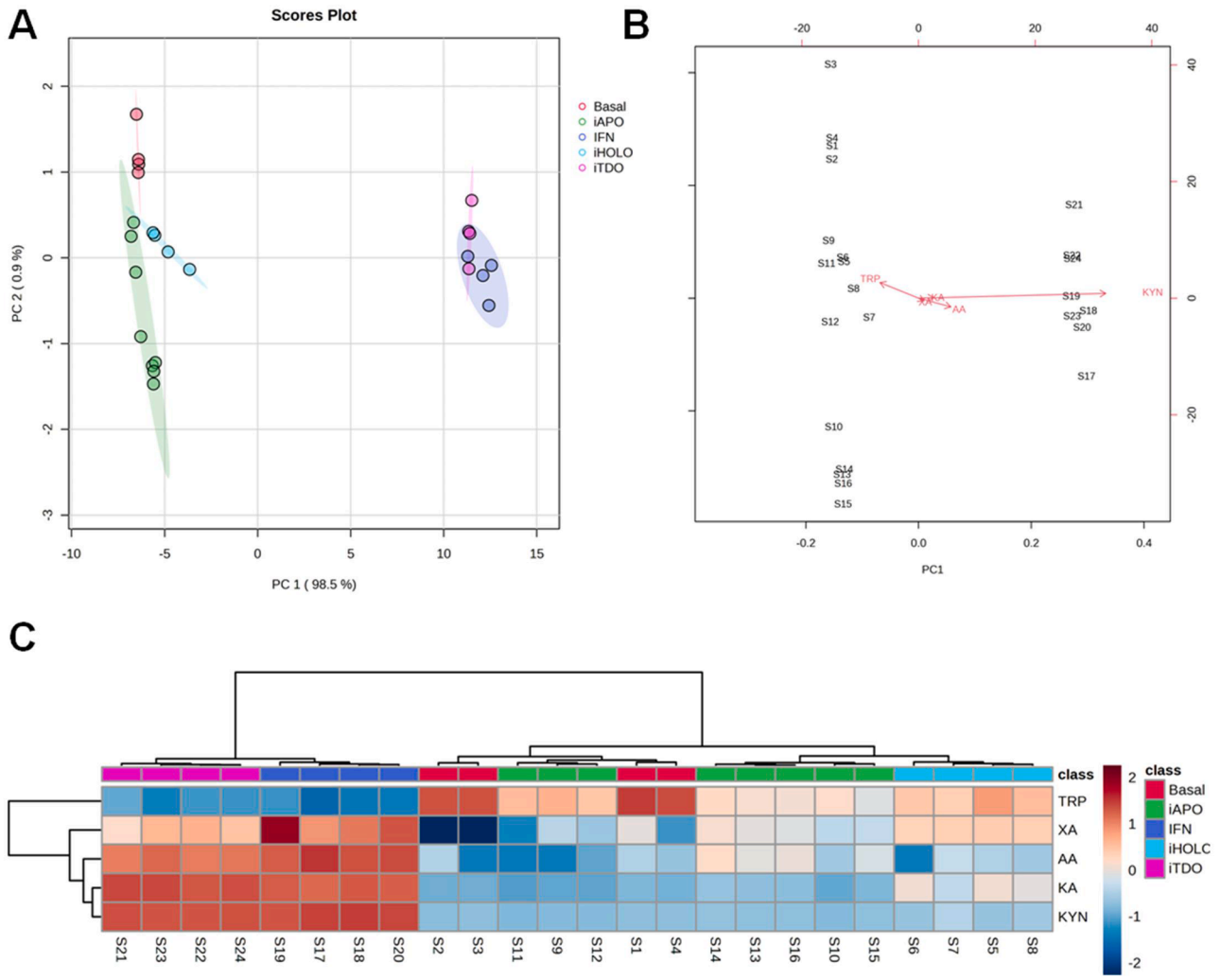

Fig. 5. Multivariate analysis in A375 cell line: Principal Component Analysis (PCA) and heatmap. (A) Score plot showing the principal component that explains 98.5% of the observed variability. Circular areas represent the 95% confidence interval (CI) for each feature. (B) Biplot displaying the monitored variables across the study samples. (C) Heatmap of metabolites, where red squares indicate high analyte concentrations and blue squares emphasize low concentrations. The heatmap is provided with clustering *via* Ward's method. The entire dataset was obtained from three independent experiments.

decreased until reaching the PC condition, which corresponds to the basal metabolic levels in the absence of IFNγ induction. The clustering obtained using Ward's method also reveals similarities between the experimental groups in the heat maps.

Overall, the observed trends in kynurenine levels and their downstream metabolites, in response to selective hIDO1 or TDO inhibition, support the potential of our methodology as a validated screening method to characterize various cellular models. The LC-MS/MS method described in this paper enabled the quantification of AA, KA, XA, TRP, and KYN; the remaining KP catabolites were not detectable in the study samples (Supporting Information, Fig. 7S-8S).

3.4. Evaluation of TDO activity

The outcome observed in U87 and MDA-MB-231 cell lines confirmed a constitutive activation of the KP in these models, due to the expression of TDO. [33,34] The high basal levels of KA and AA observed in U87 could also support this evidence. To corroborate our hypothesis, we investigated TDO activity in the three cell lines. To achieve this aim, histograms of KYN/TRP ratios corresponding to different 680C91 concentrations were generated using GraphPad software (GraphPad Prism 9.1.0) as depicted in Fig. 8A-B. Micromolar concentrations of 680C91 have been chosen deliberately to guarantee TDO inhibition, even though this molecule is a well-known inhibitor with a potency in the nanomolar range. [35] As expected, IFNγ treatment boosted the KP leading to an increase of KYN/TRP ratios under the experimental conditions. The basal levels of KYN (≈ 250 μg/L) represent the concentration of KYN introduced in the cell culture media by FBS supplementation (Fetal Bovine Serum), which is formally the 0% condition (Supporting Information, Figs. 2S, 3S). [36] As shown in Fig. 8, A375 and MDA-MB-231 cell lines did not produce KYN/TRP ratio variations under untreated conditions, but only after IFNγ-dependent induction of hIDO1. Moreover, the A375 cell line was not significantly affected by the presence of 680C91, not even after IFNγ stimulation. Surprisingly, despite the A375 cell line being commonly used for testing the *in vitro* efficacy of hIDO1 inhibitor candidates, none of the references in the literature reported either the expression of TDO or its absence in the A375 cell line, except for our paper. In fact, both the metabolomic and the RT-PCR experiments confirmed the absence of TDO in the A375 cell line (Fig. 8C). On the other hand, the U87 cell line showed higher basal levels of KYN/TRP ratio, which can be attributed to the presence of TDO, whereas MDA-MB-231 cell line is affected by 680C91 only after IFNγ treatment suggesting that the role of TDO in the production of KYN is more significant after stimulation. [35] Of note, a decrease of KYN/TRP ratios in response to the selective TDO inhibitor was observed both in MDA-MB-231 and U87 cell lines. The expression of TDO in the U87 cell

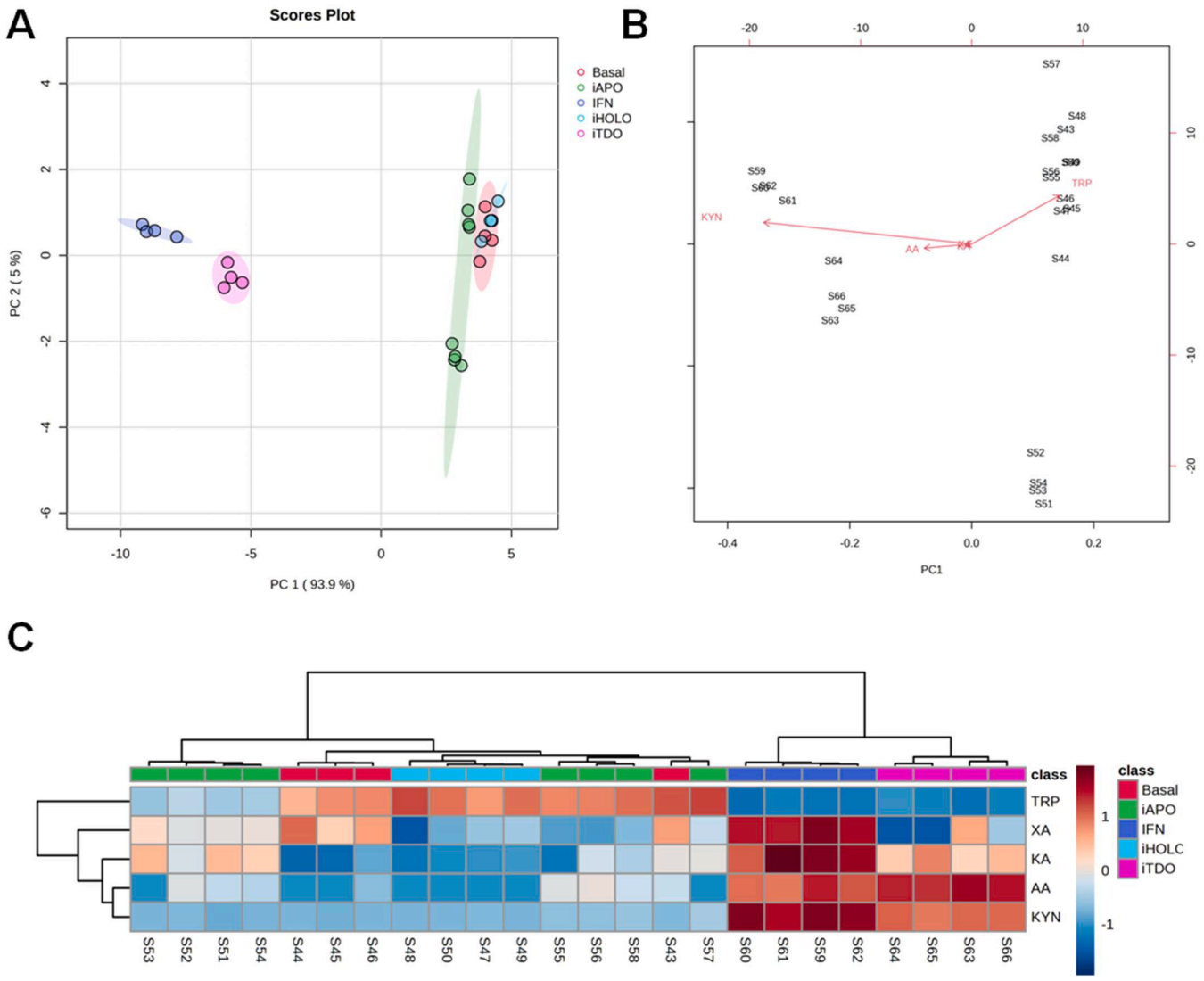

Fig. 6. Multivariate analysis in MDA-MB-231 cell line: Principal Component Analysis (PCA) and heatmap. (A) Score plot showing the principal component that explains 93.9% of the observed variability. Circular areas represent the 95% confidence interval (CI) for each feature. (B) Biplot displaying the monitored variables across the study samples. (C) Heatmap of metabolites, where red squares indicate high analyte concentrations and blue squares emphasize low concentrations. The heatmap is provided with clustering *via* Ward's method. The entire dataset was obtained from three independent experiments.

line is more evident under the CTRL conditions, probably because IFNγ induces both the upregulation of both TDO and hIDO1, which tends to mitigate the decrease of KYN concentration given by 680C91. As shown in the histograms below referred to U87 cells, after IFNγ stimulation a higher concentration of the TDO inhibitor is required to significantly reduce the KYN/TRP ratio.

Considering the basal TDO expression, the U87 cell line could be exploited in drug discovery campaigns to discern hIDO1 selective inhibitors from TDO inhibitors, since hIDO1 expression does not occur without IFNγ stimulation.

4. Conclusions

This paper introduces a validated LC-MS/MS method for quantifying KP catabolites, including TRP, KYN, XA, 3OHKYN, KA, 3OHAA, AA, 5HT, and TRYP in DMEM and EMEM cell culture media. The method demonstrates strong linearity ($r^2 > 0.99$) within a 5.0–20,000 μg/L concentration range. LLOQ values range from 5.0 to 500.0 μg/L for most compounds, except KYN, which has an LLOQ of 200 μg/L. This method offers versatility and precision across various concentration levels. Selective inhibition of both hIDO1 and TDO was investigated, and statistical analysis using Metaboanalyst 5.0 was conducted. The results were visualized through PCA analysis, heatmaps, and dendrograms and indicate that hIDO1 inhibition has a more pronounced effect on kynurenine levels compared to TDO inhibition. The heatmaps and dendrograms provided valuable insights into the relationships among the samples, highlighting distinct metabolic signatures in different cell lines. Furthermore, the analysis revealed the impact of IFNγ induction on kynurenine synthesis, with TRP acting as a trigger. The levels of TRP, KYN, and downstream metabolites varied depending on the experimental conditions and the presence of hIDO1 inhibitors. The results suggest the potential of the developed methodology as a validated screening tool for characterizing cellular models based on kynurenine levels and downstream metabolites. The lack of literature references regarding the expression or absence of TDO in the A375 cell line is surprising, considering its common use for testing hIDO1 inhibitor candidates. Our paper stands out as the exception, providing valuable information on this topic. However, additional investigations are needed to fully understand the observed trends and the differential effects of inhibitors on TRP metabolism. Overall, the study provides valuable insights into the role of hIDO1 and TDO in kynurenine metabolism and underscores the importance of further research in this area.

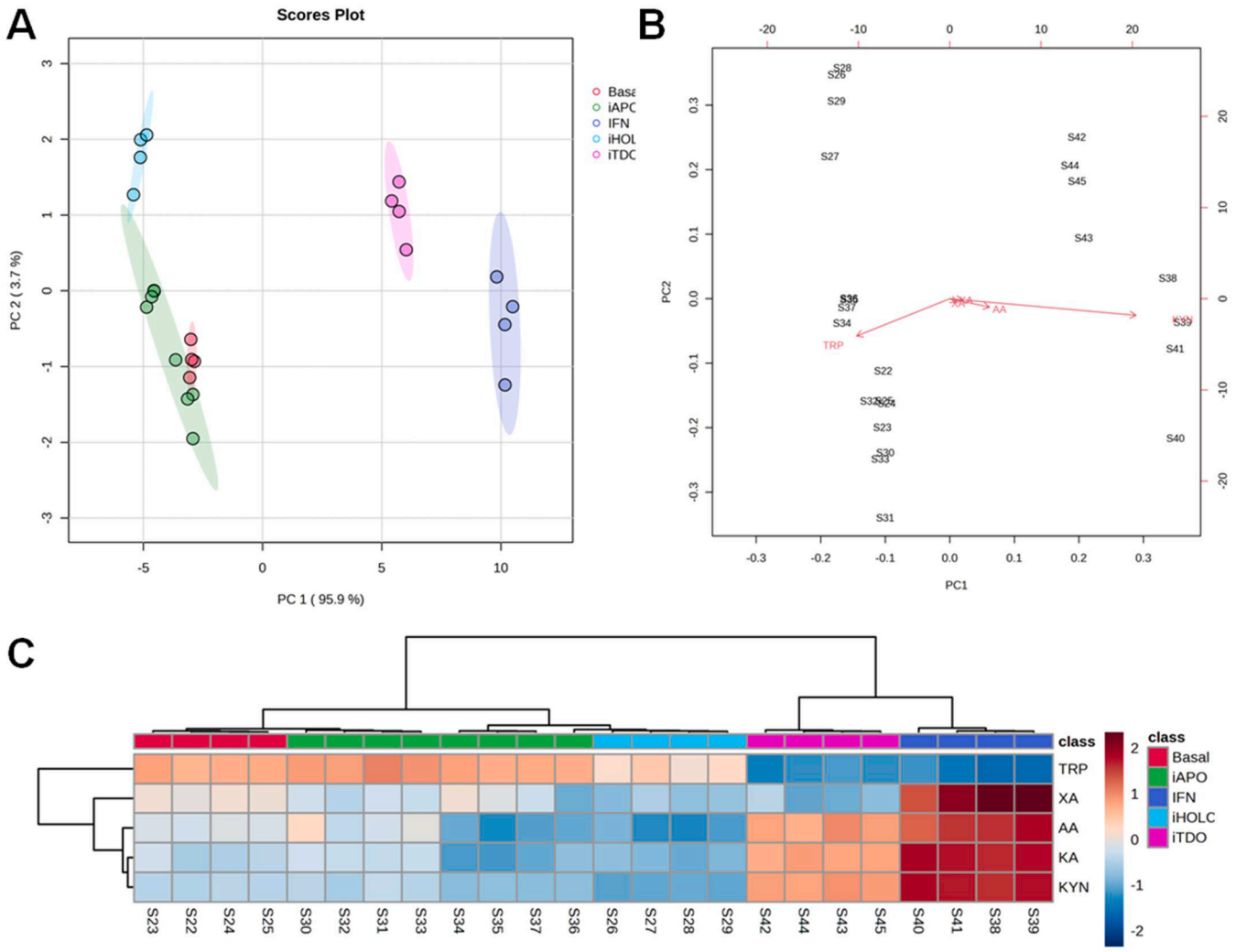

Fig. 7. Multivariate analysis in U87 cell line: Principal Component Analysis (PCA) and heatmap. (A) Score plot showing the principal component that explains 95.9% of the observed variability. Circular areas represent the 95% confidence interval (CI) for each feature. (B) Biplot displaying the monitored variables across the study samples. (C) Heatmap of metabolites, where red squares indicate high analyte concentrations and blue squares emphasize low concentrations. The heatmap is provided with clustering *via* Ward's method. The entire dataset was obtained from three independent experiments.

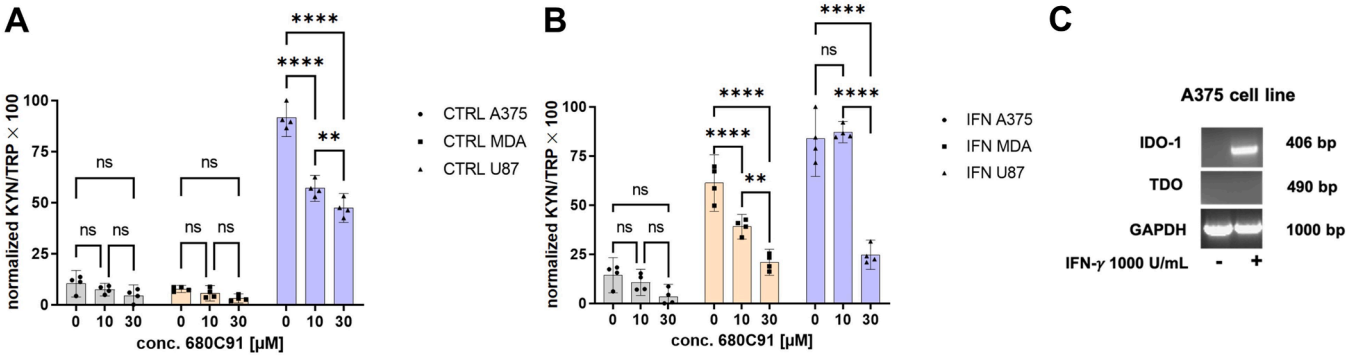

Fig. 8. Histogram representation of TDO Inhibitor-Dependent Modulation of KYN/TRP ratio. Normalized KYN/TRP ratios in culture media of A375, MDA-MB-231, and U87 cells under basal conditions (A) or IFNγ induction (B) in response to 10 and 30 μM concentrations of 6080C91 (selective TDO inhibitor). Error bars represent the mean with a 95% confidence interval (95% CI). Statistical analysis conducted using a two-way ANOVA followed by Tukey's multiple comparison test (* $p < 0.05$; ** $p < 0.01$; *** $p < 0.001$; **** $p < 0.0001$). (C) Expression of IDO and TDO mRNA by A375 cell line. IDO and TDO mRNA expression were assessed by RT-PCR on A375 cell line unstimulated/stimulated with 1000 U/mL IFNγ.

Supporting Informations

The following supporting information can be downloaded at:

Acknowledgments and funding

This work is part of the project NODES which has received funding from the MUR – M4C2 1.5 of PNRR funded by the European Union - NextGenerationEU (Grant agreement no. ECS00000036).

Institutional Review Board Statement

Not applicable, since this research involved neither humans nor animals.

CRediT authorship contribution statement

Conceptualization, E.D.G., S.F. Methodology, E.D.G., S.F. and S.V. Method Validation, S.V. Formal Analysis and Investigation, E.D.G., S.F., R.M.C.D.M., S.V. Resources E.D.G., S.F., R.M.C.D.M. Data Curation, S.V. Writing – Original Draft Preparation, S.V. Writing-Review and Editing, E.D.G., S.F., S.J.R., R.M.C.D.M., S.V., S.A. Visualization, S.V. Supervision, E.D.G., S.F. Project Administration, E.D.G. Funding Acquisition, E.D.G., R.M.C.D.M.

Declaration of Competing Interest

The authors declare that they have no known competing financial interests or personal relationships that could have appeared to influence the work reported in this paper.

Data Availability

The datasets generated during and/or analyzed during the current study are available from the corresponding author on reasonable request.

Appendix A. Supporting information

Supplementary data associated with this article can be found in the online version at doi:10.1016/j.jpba.2023.115750.

References

[1] W. Roth, K. Zadeh, R. Vekariya, Y. Ge, M. Mohamadzadeh, Tryptophan metabolism and gut-brain homeostasis, IJMS 22 (6) (2021) 2973, https://doi.org/10.3390/ijms22062973.
[2] M.T. Pallotta, S. Rossini, C. Suvieri, A. Coletti, C. Orabona, A. Macchiarulo, C. Volpi, U. Grohmann, Indoleamine 2,3–dioxygenase 1 (IDO1): an up-to-date overview of an eclectic immunoregulatory enzyme, FEBS J. 289 (20) (2022) 6099–6118, https://doi.org/10.1111/febs.16086.
[3] H.J. Ball, F.F. Fedelis, S.M. Bakmiwewa, N.H. Hunt, H.J. Yuasa, Tryptophan-catabolizing enzymes - party of three, Front. Immunol. 5 (2014), https://doi.org/10.3389/fimmu.2014.00485.
[4] A. Maeta, T. Fukuwatari, H. Funakoshi, T. Nakamura, K. Shibata, Tryptophan-restriction diets help to maintain l-tryptophan homeostasis in tryptophan 2,3-dioxygenase knockout mice, Int J. Tryptophan Res 6s1 (2013), IJTR.S12206, https://doi.org/10.4137/IJTR.S12206.
[5] A.B. Dounay, J.B. Tuttle, P.R. Verhoest, Challenges and opportunities in the discovery of new therapeutics targeting the kynurenine pathway, J. Med. Chem. 58 (22) (2015) 8762–8782, https://doi.org/10.1021/acs.jmedchem.5b00461.
[6] H.J. Yuasa, R. Stocker, Methylene blue and ascorbate interfere with the accurate determination of the kinetic properties of IDO2, FEBS J. 288 (16) (2021) 4892–4904, https://doi.org/10.1111/febs.15806.
[7] D.C. Hinshaw, L.A. Shevde, The tumor microenvironment innately modulates cancer progression, Cancer Res 79 (18) (2019) 4557–4566, https://doi.org/10.1158/0008-5472.CAN-18-3962.
[8] K. Tang, Y.-H. Wu, Y. Song, B. Yu, Indoleamine 2,3-dioxygenase 1 (IDO1) inhibitors in clinical trials for cancer immunotherapy, J. Hematol. Oncol. 14 (1) (2021), 68, https://doi.org/10.1186/s13045-021-01080-8.
[9] T.C. Mitchell, O. Hamid, D.C. Smith, T.M. Bauer, J.S. Wasser, A.J. Olszanski, J. J. Luke, A.S. Balmanoukian, E.V. Schmidt, Y. Zhao, X. Gong, J. Maleski, L. Leopold, T.F. Gajewski, Epacadostat plus pembrolizumab in patients with advanced solid tumors: phase i results from a multicenter, open-label phase i/ii trial (ECHO-202/KEYNOTE-037), JCO 36 (32) (2018) 3223–3230, https://doi.org/10.1200/JCO.2018.78.9602.
[10] S. Chen, J. Tan, A. Zhang, The ups, downs and new trends of IDO1 inhibitors, Bioorg. Chem. 110 (2021), 104815, https://doi.org/10.1016/j.bioorg.2021.104815.
[11] M.M. Hamilton, F. Mseeh, T.J. McAfoos, P.G. Leonard, N.J. Reyna, A.L. Harris, A. Xu, M. Han, M.J. Soth, B. Czako, J.P. Theroff, P.K. Mandal, J.P. Burke, B. Virgin-Downey, A. Petrocchi, D. Pfaffinger, N.E. Rogers, C.A. Parker, S.S. Yu, Y. Jiang, S. Krapp, A. Lammens, G. Trevitt, M.R. Tremblay, K. Mikule, K. Wilcoxen, J. B. Cross, P. Jones, J.R. Marszalek, R.T. Lewis, Discovery of IACS-9779 and IACS-70465 as potent inhibitors targeting indoleamine 2,3-dioxygenase 1 (IDO1) apoenzyme, J. Med. Chem. 64 (15) (2021) 11302–11329, https://doi.org/10.1021/acs.jmedchem.1c00679.
[12] H. Jia, Y. Feng, Y. Liu, X. Chang, L. Chen, H. Zhang, G. Ding, Z. Zou, Integration of 1H NMR and UPLC-Q-TOF/MS for a comprehensive urinary metabonomics study on a rat model of depression induced by chronic unpredictable mild stress, PLoS ONE 8 (5) (2013), e63624, https://doi.org/10.1371/journal.pone.0063624.
[13] Y. Qiu, G. Cai, B. Zhou, D. Li, A. Zhao, G. Xie, H. Li, S. Cai, D. Xie, C. Huang, W. Ge, Z. Zhou, L.X. Xu, W. Jia, S. Zheng, Y. Yen, W. Jia, A distinct metabolic signature of human colorectal cancer with prognostic potential, Clin. Cancer Res. 20 (8) (2014) 2136–2146, https://doi.org/10.1158/1078-0432.CCR-13-1939.
[14] I. Sadok, K. Rachwał, M. Staniszewska, Application of the optimized and validated LC–MS method for simultaneous quantification of tryptophan metabolites in culture medium from cancer cells, J. Pharm. Biomed. Anal. 176 (2019), 112805, https://doi.org/10.1016/j.jpba.2019.112805.
[15] Z. Sun, Q. Ji, A.R. Evans, M.J. Lewis, J. Mo, P. Hu, High-throughput LC-MS quantitation of cell culture metabolites, Biologicals 61 (2019) 44–51, https://doi.org/10.1016/j.biologicals.2019.07.003.
[16] Y. Simón-Manso, M.S. Lowenthal, L.E. Kilpatrick, M.L. Sampson, K.H. Telu, P. A. Rudnick, W.G. Mallard, D.W. Bearden, T.B. Schock, D.V. Tchekhovskoi, N. Blonder, X. Yan, Y. Liang, Y. Zheng, W.E. Wallace, P. Neta, K.W. Phinney, A. T. Remaley, S.E. Stein, Metabolite profiling of a NIST standard reference material for human plasma (SRM 1950): GC-MS, LC-MS NMR, and clinical laboratory analyses, libraries, and web-based resources, Anal. Chem. 85 (24) (2013) 11725–11731, https://doi.org/10.1021/ac402503m.
[17] A. Nasiri, R. Jahani, S. Mokhtari, H. Yazdanpanah, B. Daraei, M. Faizi, F. Kobarfard, Overview, consequences, and strategies for overcoming matrix effects in LC-MS analysis: a critical review, Analyst 146 (20) (2021) 6049–6063, https://doi.org/10.1039/D1AN01047F.
[18] B. Maneglier, C. Rogez-Kreuz, P. Cordonnier, P. Therond, C. Advenier, D. Dormont, P. Clayette, O. Spreux-Varoquaux, Simultaneous measurement of kynurenine and tryptophan in human plasma and supernatants of cultured human cells by HPLC with coulometric detection, Clin. Chem. 50 (11) (2004) 2166–2168, https://doi.org/10.1373/clinchem.2004.037465.
[19] Y. Qi, R. Wang, L. Zhao, L. Lv, F. Zhou, T. Zhang, F. Lu, H. Yan, G. Duan, Celastrol suppresses tryptophan catabolism in human colon cancer cells as revealed by metabolic profiling and targeted metabolite analysis, Biol. Pharm. Bull. 41 (8) (2018) 1243–1250, https://doi.org/10.1248/bpb.b18-00171.
[20] K. Yamada, T. Miyazaki, T. Shibata, N. Hara, M. Tsuchiya, Simultaneous measurement of tryptophan and related compounds by liquid chromatography/electrospray ionization tandem mass spectrometry, J. Chromatogr. B 867 (1) (2008) 57–61, https://doi.org/10.1016/j.jchromb.2008.03.010.
[21] W. Zhu, A.P. Stevens, K. Dettmer, E. Gottfried, S. Hoves, M. Kreutz, E. Holler, A. B. Canelas, I. Kema, P.J. Oefner, Quantitative profiling of tryptophan metabolites in serum, urine, and cell culture supernatants by liquid chromatography–tandem mass spectrometry, Anal. Bioanal. Chem. 401 (10) (2011) 3249–3261, https://doi.org/10.1007/s00216-011-5436-y.
[22] I. Sadok, K. Rachwał, M. Staniszewska, Simultaneous quantification of selected kynurenines analyzed by liquid chromatography-mass spectrometry in medium collected from cancer cell cultures, JoVE (159) (2020) 61031, https://doi.org/10.3791/61031.
[23] M. Serafini, E. Torre, S. Aprile, E. Del Grosso, A. Gesù, A. Griglio, G. Colombo, C. Travelli, S. Paiella, A. Adamo, E. Orecchini, A. Coletti, M.T. Pallotta, S. Ugel, A. Massarotti, T. Pirali, S. Fallarini, Discovery of highly potent benzimidazole derivatives as indoleamine 2,3-dioxygenase-1 (IDO1) inhibitors: from structure-based virtual screening to *in Vivo* pharmacodynamic activity, J. Med. Chem. 63 (6) (2020) 3047–3065, https://doi.org/10.1021/acs.jmedchem.9b01809.
[24] FDA, 2018 - Bioanal. Method Valid. Guid. Ind. (2018). https://www.fda.gov/files/drugs/published/Bioanalytical-Method-Validation-Guidance-for-Industry.pdf (Accessed 8 March 2022).
[25] Committee for Medicinal Products for Human Use (CHMP), Eur. Med. Agency (EMA). EMA 2011 - Guidel. Bioanal. Method Valid. (2011). https://www.ema.europa.eu/en/documents/scientific-guideline/guideline-bioanalytical-method-validation_en.pdf (Accessed 8 March 2022).
[26] ICH guideline M10 on bioanalytical method validation and study sample analysis. https://www.ema.europa.eu/en/documents/scientific-guideline/ich-guideline-m10-bioanalytical-method-validation-step-5_en.pdf.
[27] R. Canavesi, R. Miggiano, M. Stella, U. Galli, F. Rossi, M. Rizzi, E. Del Grosso, Study of Anopheles gambiae 3-hydroxykynurenine transaminase activity and inhibition by LC-MS/MS method, J. Pharm. Biomed. Anal. 173 (2019) 154–161, https://doi.org/10.1016/j.jpba.2019.05.025.
[28] V. Bortolotto, F. Mancini, G. Mangano, R. Salem, E. Xia, E. Del Grosso, M. Bianchi, P.L. Canonico, L. Polenzani, M. Grilli, Proneurogenic effects of trazodone in murine

and human neural progenitor cells, ACS Chem. Neurosci. 8 (9) (2017) 2027–2038, https://doi.org/10.1021/acschemneuro.7b00175.
[29] W. Zhou, S. Yang, P.G. Wang, Matrix effects and application of matrix effect factor, Bioanalysis 9 (23) (2017) 1839–1844, https://doi.org/10.4155/bio-2017-0214.
[30] I.R. Pizzutti, J.V. Dias, A. de Kok, C.D. Cardoso, G.M.E. Vela, Pesticide residues method validation by UPLC-MS/MS for accreditation purposes, J. Braz. Chem. Soc. (2016), https://doi.org/10.5935/0103-5053.20160012.
[31] B.K. Matuszewski, Standard line slopes as a measure of a relative matrix effect in quantitative HPLC–MS bioanalysis, J. Chromatogr. B 830 (2) (2006) 293–300, https://doi.org/10.1016/j.jchromb.2005.11.009.
[32] A. Brittoli, S. Fallarini, H. Zhang, R.J. Pieters, G. Lombardi, In Vitro" studies on galectin-3 in human natural killer cells, Immunol. Lett. 194 (2018) 4–12, https://doi.org/10.1016/j.imlet.2017.12.004.
[33] N.C. D'Amato, T.J. Rogers, M.A. Gordon, L.I. Greene, D.R. Cochrane, N. S. Spoelstra, T.G. Nemkov, A. D'Alessandro, K.C. Hansen, J.K. Richer, A TDO2-AhR signaling axis facilitates anoikis resistance and metastasis in triple-negative breast cancer, Cancer Res. 75 (21) (2015) 4651–4664, https://doi.org/10.1158/0008-5472.CAN-15-2011.
[34] S. Zhang, F. Qi, X. Fang, D. Yang, H. Hu, Q. Huang, C. Kuang, Q. Yang, Tryptophan 2,3-dioxygenase inhibitory activities of tryptanthrin derivatives, Eur. J. Med. Chem. 160 (2018) 133–145, https://doi.org/10.1016/j.ejmech.2018.10.017.
[35] M. Salter, R. Hazelwood, C.I. Pogson, R. Iyer, D.J. Madge, The effects of a novel and selective inhibitor of tryptophan 2,3-dioxygenase on tryptophan and serotonin metabolism in the rat, Biochem. Pharmacol. 49 (10) (1995) 1435–1442, https://doi.org/10.1016/0006-2952(95)00006-L.
[36] U.M. Litzenburger, C.A. Opitz, F. Sahm, K.J. Rauschenbach, S. Trump, M. Winter, M. Ott, K. Ochs, C. Lutz, X. Liu, N. Anastasov, I. Lehmann, T. Höfer, A. von Deimling, W. Wick, M. Platten, Constitutive IDO expression in human cancer is sustained by an autocrine signaling loop involving IL-6, STAT3 and the AHR, Oncotarget 5 (4) (2014) 1038–1051, https://doi.org/10.18632/oncotarget.1637.